Nanochem Res 2026, 11(1): 152-168
10.22036/ncr.2025.527594.1486

RESEARCH PAPER

Green Synthesis of ZnO Nanoparticles Using *Antidesma Orthogyne* Extract and Their Antimicrobial and Cytotoxic Activities

Muhammad Taher[1]*, Nik Mawaddah Nik Abd Rahman Zaki[1], Juliana Md Jaffri[1], Deny Susanti[2], Junaidi Khotib[3]**, Md. Faiyazuddin[4], Muhammad Salahuddin Haris[5]

[1] Department of Pharmaceutical Technology, Kulliyyah of Pharmacy, International Islamic University Malaysia, Jalan Sultan Ahmad Shah, 25200 Kuantan, Pahang, Malaysia.
[2] Department of Chemistry, Faculty of Science, International Islamic University Malaysia, Jalan Sultan Ahmad Shah, 25200 Kuantan, Pahang, Malaysia.
[3] Department of Pharmacy Practice, Faculty of Pharmacy, Airlangga University, 60115, Surabaya, Indonesia.
[4] Centre for Global Health Research, Saveetha Institute of Medical and Technical Sciences, Tamil Nadu, Chennai, India.
[5] Department of Pharmacy, Faculty of Pharmacy and Health Sciences, Royal College of Medicine Perak, Universiti Kuala Lumpur, 30450 Ipoh, Perak, Malaysia.

Received: 2025-06-01 Revised: 2025-07-14 Accepted: 2025-07-26

HIGHLIGHTS

- Biogenic synthesis of ZnO nanoparticles
- Phytochemicals mediated green synthesis
- Potential use of nanoparticles in biomedical applications

ABSTRACT

The green synthesis approach using plant extracts is preferable due to its effectiveness in producing nanoparticles (NPs). In this study, *Antidesma orthogyne* leaf extract was used to synthesize ZnO-NPs. Phytochemical profiling was conducted using liquid chromatography- mass spectrometry quadrupole time-of-flight, and the synthesized ZnO-NPs were characterized using UV-Vis spectroscopy, dynamic light scattering, zeta potential, scanning electron microscopy (SEM), energy dispersive X-ray (EDX), Fourier transform infrared spectroscopy (FTIR), X-ray diffraction (XRD), and thermogravimetric analysis (TGA). Antimicrobial activity was evaluated against selected microorganisms using the disc diffusion method, while cytotoxicity was assessed on MCF-7 human epithelial breast adenocarcinoma cells via MTT assay. The results showed that pH 12 was the optimal condition for ZnO-NP synthesis, yielding NPs with an average size of 131.1 nm and an absorption peak at 351 nm. SEM images indicated slight aggregation, while XRD patterns confirmed the hexagonal wurtzite structure of ZnO-NPs. FTIR and EDX analyses confirmed the formation of ZnO-NPs, and TGA demonstrated thermal stability up to 700°C. In terms of antimicrobial and cytotoxic activities, the ZnO-NPs exhibited notable activities in both assays. Hence, these findings suggest that *A. orthogyne* extract effectively facilitates ZnO-NP synthesis, producing NPs with potential biomedical applications.

KEYWORDS: *Green Synthesis, Antidesma, Zinc Oxide Nanoparticles, Antibacterial, Cytotoxicity*

How to cite this article
Taher M, Nik Abd Rahman Zaki N M, Md Jaffri J, Susanti D, Khotib J, Faiyazuddin MD, Haris M S, Green Synthesis of ZnO Nanoparticles Using Antidesma orthogyne Extract and Their Antimicrobial and Cytotoxic Activities. Nanochem Res, 2026 11(1): 152-168, DOI: 10.22036/ncr.2025.527594.1486

* **Corresponding Author:** Email: mtaher@iium.edu.my
** **Corresponding Author:** Email: junaidi-k@ff.unair.ac.id

1. INTRODUCTION

Antimicrobial resistance (AMR) has become one of the major global health issues and threats to human life. According to the World Health Organisation (WHO), around 1.27 million deaths in 2019 were caused by microbial resistance [1]. Not only that, the Global Antimicrobial Resistance and Use Surveillance System (GLASS) 2022 also reported more than a 15% increase in the rate of AMR in 2020 after the emergence of Covid-19 for several antimicrobial agents, including third-generation cephalosporins, which are the first-line empirical therapy for bloodstream infection [2]. AMR is a natural process that happens when antimicrobial agents are no longer able to kill the bacteria, viruses, fungi, or parasites causing the infection via genetic alteration in the pathogen. However, the widespread misuse and overuse of antimicrobials have accelerated this process [1], causing the microorganisms to develop resistance easily towards antimicrobial agents.

Over the past decades, there has been an increase in the amount of biofilm formation among multidrug-resistant bacteria [3]. A biofilm is a self-produced complex matrix in which bacteria cells are embedded, protecting them from harsh environments, including antimicrobials [4,5]. Nanoparticles, which are small objects within the range of 1–100 nm in diameter, were reported to have a variety of modes of antimicrobial activity, especially in combating biofilm formation due to their unique physicochemical properties, surface charge, and small size [6]. Specifically, metal oxide nanoparticles were found to exhibit promising antimicrobial activity with potential bactericidal and antibiofilm effects [5], primarily due to oxidative stress caused by the formation of reactive oxygen species (ROS) [7]. Numerous types of metals have been identified to possess antimicrobial properties, including aluminium, silver, cadmium, ferrous, zinc, and a few more metals [8]. Zinc oxide nanoparticles (ZnO-NPs) are one of the most studied metals among them due to their biocompatibility, lower toxicity, lower cost, and predominant antimicrobial activities [9,10].

Nowadays, the green synthesis approach is preferable due to its proven effectiveness, eco-friendliness, cost-efficiency, safety, and large-scale productivity in producing NPs with good properties. Plant extracts have been discovered to act as bio-reducing and capping agents that assist the synthesis of NPs [11,12]. The presence of diverse phytoconstituents in plants, particularly those with antioxidant effects like phenolics and flavonoids, was found to be responsible for these activities. The *Antidesma* genus is one of the potential plants that may facilitate this NP synthesis, owing to its diverse array of phytochemicals. More than 140 phytochemicals have been reported from this genus, including alkaloids, phenolics, flavonoids, and many more [13]. Therefore, in this study, we aim to explore the potential of *A. orthogyne* (Fig. 1) leaf extract to mediate the synthesis of ZnO-NPs, characterize their properties, and evaluate their antimicrobial and cytotoxic activities.

2. MATERIALS AND METHODS

2.1. Materials

Fresh *A. orthogyne* leaves were collected in Kuantan, Pahang, Malaysia, in October 2024 and were identified by Dr Shamsul Khamis. The plant specimen was deposited at the Herbarium of Kulliyyah of Pharmacy, IIUM. Cell lines and microbes were obtained from ATCC, US, methanol (Merck), zinc nitrate hexahydrate ($Zn(CH_3COO)_2.2H_2O$) powder (Sigma-Aldrich), sodium hydroxide pellets (R&M Chemicals), nutrient broth powder, nutrient agar powder, Tryptone Soya broth powder, Tryptone Soya agar powder, Dulbecco's Modified Eagle's Medium (DMEM) (Gibco), 10% foetal bovine serum (Gibco), Penicillin-Streptomycin Mixed solution (Nacalai Tesque), TrypLE Express (Gibco), phosphate-buffered saline

Fig. 1 *A. orthogyne leaves* and fruits collected at Kuantan, Pahang, Malaysia

(PBS) (Sigma-Aldrich), 3-(4,5-dimethylthiazol-2-yl)-2,6-diphenyltetrazolium bromide (MTT) (Molecular probes), dimethyl sulphoxide (DMSO) (Supelco), amoxicillin/clavulanic acid discs (Oxoid), econazole nitrate, tamoxifen citrate, analytical balance, pH meter, drying cabinet, mechanical grinder, refrigerator, sonicator probe (Qsonica sonicator probe), rotary evaporator (Buchi Rotavapor R-100), high speed centrifuge, magnetic stirrer with heating plate, oven, autoclave, incubator, CO_2 incubator, Liquid Chromatography Mass Spectrometry Quadrupole Time-of-Flight (LC/MS-QTOF) (Agilent 1200), UV-Vis spectroscopy (UV-1800 Shimadzu UV Spectrophotometer), dynamic light scattering (DLS) and zeta potential analysis (Malvern Zetasizer Nano series), scanning electron microscopy (SEM) (JEOL/JSM-IT200), energy dispersive X-ray (EDX) (ZEISS EVO 50), Fourier transform infrared spectroscopy (FTIR) (PerkinElmer Spectrum Two), X-ray diffraction (XRD) (PANalytical/X'Pert^3 Powder), and thermo-gravimetric analysis (TGA) (Hitachi/ STA7000).

2.2. METHODOLOGY

2.2.1. Preparation of A. orthogyne Leaf Extract

Firstly, the fresh *A. orthogyne* leaves were washed thoroughly with tap water several times to remove any dust and impurities before being dried in a drying cabinet at 40°C for six days. After that, the dried leaves were shredded and ground to a coarse powder using a mechanical grinder and stored in an airtight glass bottle in a cool and dry environment. The extraction process was conducted via the ultrasound-assisted extraction method [14]. 50 mg of the pulverized *A. orthogyne* leaves were added to 500 mL of methanol/water (70/30 v/v) in a beaker. Then, the mixture was extracted using a sonicator probe (Qsonica) at the amplitude of 60 kHz for 30 minutes with the temperature not exceeding 50°C. After that, the mixture was filtered using filter paper and a 0.22 µm syringe filter into a volumetric flask before being stored in a cold and dark environment for the next use.

2.2.2. Liquid Chromatography Mass Spectrometry Quadrupole Time-of-Flight (LC/MS-QTOF) Analysis

Before conducting the LC/MS analysis, the *A. orthogyne* extract was dried under vacuum using a Buchi Rotavapor R-100 at 50°C, 130 rpm, and 90-150 mbar vacuum. The concentrated extract was diluted in methanol to 1 mg/mL, then filtered using a 0.22 µm pore size syringe filter. For LC/MS analysis, an Agilent ZORBAX Eclipse Plus C18 Rapid Resolution HT (2.1 x 100 mm) 1.8 µm column with a gradient elution program was utilized. The mass spectrometry was performed in positive electrospray ionisation (ESI) mode. Lastly, the data were analyzed using Agilent Mass Hunter Qualitative Analysis B.05.00 software.

2.2.3. Synthesis of ZnO-NPs

This synthesis procedure was adapted from prior studies with a few adjustments. 0.1 M zinc nitrate hexahydrate ($Zn(CH_3COO)_2.2H_2O$) solution was prepared by dissolving 2.975 g of ($Zn(CH_3COO)_2.2H_2O$) powder into 100 mL of distilled water. 10 mL of *A. orthogyne* extract was added dropwise using a burette to the zinc nitrate solution, which was stirred under magnetic conditions at 800 rpm and maintained at 55-65°C for 2 hours [10,15]. Then, the pH was adjusted to pH 12 by adding 1 M NaOH solution before continuing the synthesis under the same conditions for another 1 hour [16]. The formation of a cream-coloured zinc hydroxide precipitate was observed. The mixture was allowed to sit for 30 min before being centrifuged at 10,000 rpm for 10 min. After removing the supernatant, the pellets were rinsed by re-dispersions in distilled water and then centrifuged. The rinsing process was repeated three times. Lastly, the pellets were dried in an oven at 50°C for 24 hours and stored in an airtight container for further analysis. This synthesis was repeated at pH 7, pH 9, and without the addition of NaOH.

2.2.4. Characterisation of the Synthesized ZnO-NPs

The synthesized NPs were characterized by using different techniques, including UV-visible spectroscopy, dynamic light scattering (DLS), zeta potential analysis, scanning electron microscopy (SEM), energy dispersive X-ray (EDX), Fourier transform infrared (FTIR) spectroscopy, X-ray diffraction (XRD), and thermogravimetric analysis (TGA). For UV-Vis analysis, 1 mL of the NPs suspension was collected at the end of the reaction and further diluted in distilled water in a 1:100 ratio. The spectra were recorded over the 200–800 nm wavelength range to confirm the formation of ZnO-NPs using the UV-1800 Shimadzu UV Spectrophotometer. DLS and zeta potential analysis were conducted using the Malvern Zetasizer Nano series to determine the hydrodynamic size, dispersion, and stability of the ZnO-NPs in their colloidal solution. These analyses were conducted using the same colloidal samples from UV-Vis analysis. SEM analysis was employed to observe the surface morphology and measure the size of the NPs, while EDX analysis was performed to analyse their elemental composition. Fourier Transform Infrared (FTIR) spectroscopy was conducted using PerkinElmer Spectrum Two, at 4000-400 cm^{-1} using the attenuated total reflectance (ATR) method, to identify the surface functional groups as well as stretching and bending vibrations of the ZnO-NPs, aiding in determining the possible phytochemicals that are responsible as bio-reducing and capping agents during the synthesis as well as confirming the formation of ZnO-NPs. XRD analysis was performed to analyse the crystalline structure and size of the NPs using PANalytical/X'Pert3 Powder. TGA was conducted by heating the sample between 30°C and 700°C at a 10°C/min heating rate under N_2 airflow using Hitachi/STA7000 to determine its thermal stability. All these analyses were performed using the dried ZnO-NPs.

10.22036/ncr.2025.527594.1486
Nanochem Res, 2026, 11(1): 152-168

2.2.5. Antimicrobial Activity of the Synthesized ZnO-NPs

The antimicrobial activity of the synthesized ZnO-NPs was evaluated against two Gram-positive bacteria (*Staphylococcus aureus* and *Bacillus subtilis*), two Gram-negative bacteria (*Escherichia coli* and *Pseudomonas aeruginosa*), and one fungal strain (*Candida albicans*) using the disc diffusion method [17,18]. Prior to the assay, the bacteria and fungi were cultured for 24 hours. The bacteria were cultured on nutrient agar and incubated at 37 ± 1°C, while *Candida* was on tryptic soy agar at 35 ± 1°C. On the following day, the fresh microorganisms were inoculated into their respective broths and standardized to 0.5 McFarland standard using a UV spectrophotometer, targeting an absorbance reading of 0.08-0.1 at 625 nm. Then, the standardized microbial suspensions were swabbed onto their respective agar plates. Sterile 6 mm discs were loaded with the following samples: ZnO-NPs (0.5, 1, 3, and 5 mg/mL), *A. orthogyne* extract (5 mg/mL), zinc nitrate hexahydrate solution (5 mg/mL), amoxicillin and clavulanic acid (30 µg/disc) as a positive control for bacteria, econazole (100 µg/mL) as a positive control for fungi, and distilled water as a negative control, before being placed onto the agar plates. The plates were incubated at 37 ± 1°C for 24 hours for bacteria and at 35 ± 1°C for 120 hours for fungi. The diameter of the inhibition zones surrounding each disc was measured in millimetres and recorded. The assay was performed in duplicate.

2.2.6. Cytotoxic Effects of the Synthesized ZnO-NPs

This cytotoxic assay procedure was adapted from previous studies with some modifications [19]. The activity was evaluated on human epithelial breast adenocarcinoma cells (MCF-7) using 3-(4,5-dimethylthiazol-2-yl)-2,6-diphenyl-tetrazolium bromide (MTT) assay. The cells were cultured in Dulbecco's Modified Eagle's Medium (DMEM) supplemented with 10% foetal bovine serum, 100 U/mL penicillin, and 100 µg/mL streptomycin and maintained at 37°C in a 5% CO_2 incubator.

For the assay, 100 µL of DMEM containing 2.0 × 10^4 cells/well was seeded into a tissue culture 96-well plate and incubated overnight at 37°C to allow for cell attachment. Then, after removing the DMEM and rinsing the wells twice using PBS, the cells were treated with 100 µL of the samples and further incubated for another 24 hours at 37°C. The samples included ZnO-NPs, zinc nitrate hexahydrate, tamoxifen (as a positive control), and plant extract. All samples, except for plant extract and negative control, were prepared in serial dilutions (1, 0.5, 0.25, 0.125, 0.06, and 0.03 mg/mL) for comparison. Following treatment, the media were removed, and the wells were rinsed again. 10 µL of MTT solution (5 mg/mL) was added into each well together with 90 µL of fresh DMEM and re-incubated for 4 h. After that, 100 µL of dimethyl sulfoxide (DMSO) was introduced, followed by another 30 minutes of incubation to dissolve the formazan crystals. Lastly, the absorbance was measured at 570 nm using DMSO as the blank.

All treatments were conducted in triplicate, and each absorbance reading was recorded three times to ensure its accuracy and consistency. The average absorbance values were then used to calculate the percentage of cell viability and percentage of inhibition using the following equations (1) and (2).

$$\% \text{ Cell Viability} = \frac{Absorbance\ of\ treated\ sample - Absorbance\ of\ blank}{Absorbance\ of\ control - Absorbance\ of\ blank} \times 100 \quad (1)$$

$$\% \text{ Inhibition} = \frac{Absorbance\ of\ control - Absorbance\ of\ treated\ sample}{Absorbance\ of\ control} \times 100 \quad (2)$$

2.2.7. Statistical Analysis

The antimicrobial and cytotoxicity data were obtained from replicated experiments and reported as mean values with standard deviation (mean ± SD). The cytotoxic activity was statistically analysed using one-way ANOVA via SPSS software (Jamovi), and IC_{50} values were calculated using linear regression. A probability value of less than 0.05 ($p < 0.05$) was considered as statistically significant [20,21]. For the antimicrobial activity, statistical analysis was not performed due to the limited number of replicates.

3. RESULTS AND DISCUSSION

3.1. Phytochemicals of A. orthogyne

The LC/MS-QTOF analysis of *A. orthogyne* leaf methanolic extract successfully detected around 500 types of compounds (Fig. 2). Among them, the notable compounds are choline, 11-deacetylvaltrate 11-(3-hydroxy-3-methylbuta-noate), 5-cholestene-3β,7α,12α,24-tetrol, 2-ethyl-dodecanoic acid, trans-resveratrol-d4, C16 sphinganine, 16-hydroxy hexadecanoic acid, 8,8-diethoxy-2,6-dimethyl-2-octanol, emmotin A, and docosanedioic acid. Table 1 shows the most abundant identified compounds in the extract. These compounds belong to various phytochemical classes, including alkaloids, polyphenols, terpenoids, flavonoids, amino acids, fatty acids and sterols. Previous studies on *Antidesma* genus plants have reported the presence of alkaloids, phenols, flavonoids, lignans, and terpenoids [13]. The high phenolic content in *Antidesma* genus has been associated with its notable antioxidant activity [13], which is believed to facilitate the reduction process in ZnO-NPs synthesis through ROS and free-radical neutralization, as well as metal ion chelation [22]. Hence, the *A. orthogyne* leaf extract is also believed to possess the potential to aid the formation of

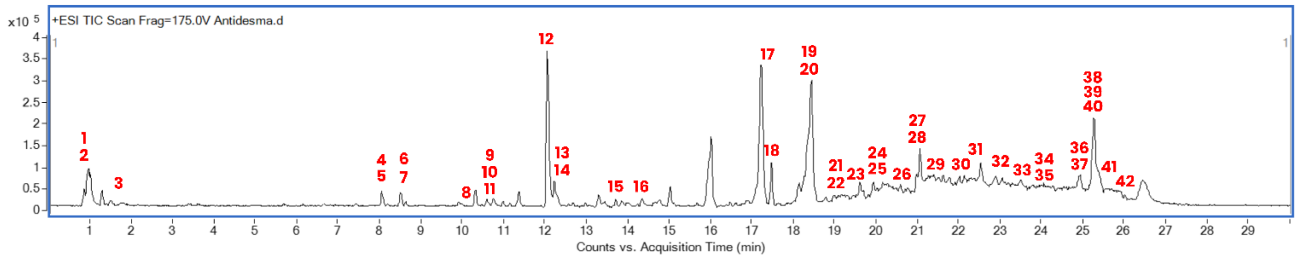

Fig. 2 LC/MS-QTOF spectra of methanolic A. orthogyne leaf extract, with numbered peaks corresponding to the compounds listed in **Table 1.** The analysis was conducted using 2 µL of sample (1 mg/mL, diluted in methanol), separated via liquid chromatography with deionized water and acetonitrile as mobile phase, under gradient elution program: 0.00-18.00 min (5-95%), 18-23 min (95%), and 23.01-30 min (5%). The mass spectrometer was operated in positive electrospray ionization (ESI) mode).

ZnO-NPs.

Nevertheless, even though hundreds of compounds were identified in this analysis, only half of them were previously reported, while the rest remain unknown. Notably, some of these unknown compounds were detected in substantial quantities, suggesting their possible involvement in the reducing and capping activities observed in the present ZnO-NPs synthesis.

3.2. Synthesis of ZnO-NPs

The synthesis was performed under four different pH conditions: pH 7, pH 9, pH 12 and without NaOH (~pH 3.24), to determine the optimum pH for ZnO-NPs synthesis. The selection was made based on the NP size, dispersion and physicochemical properties [23]. During synthesis, the appearance of a white-cream precipitate indicated the formation of ZnO-NPs, which are chemically white in colour. The reaction mixture also exhibited a gradual colour change from light yellowish-brown to light brown over time (Fig. 3). Notably, a rapid and significant colour change was observed after pH adjustment (Fig. 3 (c,d,e)), suggesting accelerated ZnO-NPs formation due to the high amount of hydroxide (OH^-) ions from NaOH, which also facilitates the formation of ZnO [24]. In contrast, minimal white-cream precipitates were observed in the synthesis conducted without NaOH (Fig. 3 (f)), which may indicate limited NPs formation under acidic conditions via plant extract alone.

After synthesis, the mixture was centrifuged and rinsed with distilled water to remove residual impurities before drying (Fig. 4). As shown in Table 2, the total dry yield increased with pH, with pH 12 producing the highest yield, and the synthesis without NaOH resulted in the lowest yield. This trend is likely due to the greater availability of OH ions at higher pH, which enhance ZnO-NPs formation. Previous studies have reported that pH may influence the shape, size and synthesis rate of NPs [25] by promoting nucleation centers and increasing the reduction of zinc ions to ZnO-NPs [26]. Moreover, pH also affects the interaction between zinc ions and the plant's functional groups, shortening the reaction time and allowing more NPs to form [26]. Hence, this may explain the higher yields observed in the presence of NaOH.

On the other hand, the low yield observed in the absence of NaOH may suggest the lack of functional groups or compounds in *A. orthogyne* extract that are capable of reducing zinc ions to ZnO-NPs. However, further studies are required to confirm this observation by evaluating the influence other variables such as temperature, concentration of zinc precursor, and plant extract, as well as their ratios.

3.3. Characterisations of the synthesized ZnO-NPs

3.3.1. UV-Vis spectroscopy

UV-Vis analysis was carried out at 30-minute intervals during synthesis to monitor the formation of ZnO-NPs. Fig. 5 shows the UV-Vis spectra of the synthesized ZnO-NPs at every 30-minute interval and under different pH conditions. During the first 2 hours (prior to pH adjustment), the absorption peak was observed around 265 nm, with increasing intensity over time, indicating progressive ZnO-NPs formation. After pH adjustment, the peak shifted to approximately 351 nm for all pH conditions, except for the synthesis conducted without the addition of NaOH (Fig. 6). Even though ZnO-NPs are usually reported to exhibit a light absorption in the range of 360-380 nm [9,10], other studies also reported absorption peaks at 240 nm and 284 nm [10,27]. Hence, the observed absorption peaks in this study confirmed the formation of ZnO-NPs.

3.3.2. DLS and zeta potential analysis

DLS analysis revealed a well-dispersed ZnO-NPs suspension within the nanoscale range. As shown in Table 3, the particle size and polydispersity index (PDI) decreased with increasing

10.22036/ncr.2025.527594.1486
Nanochem Res, 2026, 11(1): 152-168

Table 1. Identified compounds with substantial composition from LC/MS-QTOF analysis of A. orthogyne methanolic leaf extract

No.	Compound name	Formula	RT	m/z	Type of Compound
1.	Choline	$C_5H_{14}NO$	0.936	104.1071	Choline (basic constituent of lecithin)
2.	Betaine	$C_5H_{12}NO_2$	0.971	118.0868	Amino acid
3.	Sanguisorbic acid dilactone	$C_{21}H_{10}O_{13}$	1.767	471.0182	Trihydroxybenzoic acid
4.	Decyl acetate	$C_{12}H_{24}O_2$	8.062	218.2106	Carboxylic ester
5.	11-Deacetylvaltrate 11-(3-hydroxy-3-methylbutanoate)	$C_{25}H_{36}O_9$	8.078	498.2686	Iridoid monoterpenoid
6.	1,2-Benzisothiazol-3(2H)-one	C_7H_5NOS	8.507	152.0159	Organonitrogen heterocyclic
7.	5-Cholestene-3β,7α,12α,24-tetrol	$C_{27}H_{46}O_4$	8.51	457.3291	Steroid
8.	2-ethyl-dodecanoic acid	$C_{14}H_{28}O_2$	10.295	246.2418	Medium-chain fatty acid
9.	Erythro-Bupropion	$C_{13}H_{20}ClNO$	10.6	264.1127	Aromatic ketone
10.	Trans-Resveratrol-d4	$C_{14}H_8D_4O_3$	10.748	233.1102	Phenolic compound (flavonoids)
11.	Amphibine B	$C_{39}H_{47}N_5O_5$	10.769	666.3647	Cyclopeptide alkaloid
12.	C16 Sphinganine	$C_{16}H_{35}NO_2$	12.059	274.2736	Sphingoid (aminodiol)
13.	Phytosphingosine	$C_{18}H_{39}NO_3$	12.227	318.2998	Sphingoid (amino alcohol, triol)
14.	16-hydroxy hexadecanoic acid	$C_{16}H_{32}O_3$	12.289	290.2684	Omega-hydroxy-long-chain fatty acid
15.	Enigmol	$C_{18}H_{39}NO_2$	13.863	302.3044	Amino alcohol
16.	Lys Lys Thr	$C_{16}H_{33}N_5O_5$	14.347	393.2833	Peptide
17.	8,8-Diethoxy-2,6-dimethyl-2-octanol	$C_{14}H_{30}O_3$	17.205	247.2259	Tertiary alcohol
18.	4-Hydroxyphenylacetyl- glutamine	$C_{13}H_{15}NO_6$	17.475	282.0965	Glutamic acid and derivatives
19.	Emmotin A	$C_{16}H_{22}O_4$	18.256	279.1596	Tetralins
21.	Polidocanol	$C_{30}H_{62}O_{10}$	19.049	600.4668	Alkyl polyglycol ether of lauryl alcohol (polyethylene glycols)
22.	DG(14:0/0:0/14:0) (d5)	$C_{31}H_{55}D_5O_5$	19.111	556.4395	Glycerol derivatives
23.	1a,1b-dihomo-PGE1	$C_{22}H_{38}O_5$	19.687	383.2773	Prostaglandin E1 (PGE1)
24.	N-Benzoylaspartic acid	$C_{11}H_{11}NO_5$	19.926	238.0707	Aspartic acid derivative
25.	Oleamide	$C_{18}H_{35}NO$	20.027	304.2615	Fatty amide derived from oleic acid
26.	Palmityl Trifluoromethyl Ketone	$C_{17}H_{31}F_3O$	20.769	309.2409	Analog of palmitic acid
27.	Dodemorph	$C_{18}H_{35}NO$	20.984	282.2784	Morpholines
28.	24-Nor-5β-cholane-3α,7α,12α,22,23-pentol	$C_{23}H_{40}O_5$	21.065	397.2936	Bile acid
29.	DG(15:0/0:0/15:0) (d5)	$C_{33}H_{59}D_5O_5$	21.287	584.4715	Glycerolipids
30.	2,3,4'-Trihydroxy-4-Methoxybenzophenone	$C_{14}H_{12}O_5$	22.007	278.1018	Benzophenones
31.	N-stearoyl valine	$C_{23}H_{45}NO_3$	22.302	384.3458	N-acylamides (valine derivatives)
33.	Stearamide	$C_{18}H_{37}NO$	23.048	284.2939	Fatty amide of stearic acid
34.	Xanthotoxol glucoside	$C_{17}H_{16}O_9$	23.497	403.0418	Glycoside (coumarins)
35.	4-(2,6,6-Trimethylcyclohex-1-enyl) but-2-en-4-one	$C_{13}H_{20}O$	24.034	193.1578	Enones compound
36.	Euphornin	$C_{33}H_{44}O_9$	24.146	607.2895	Macrocyclic diterpenoids
37.	13,14-dihydroxy-docosanoic acid	$C_{22}H_{44}O_4$	24.921	395.3118	Long-chain fatty acid.
38.	Arginyl-Phenylalanine	$C_{15}H_{23}N_5O_3$	25.162	360.1438	Dipeptide
39.	Alpha-tocopheronolactone	$C_{16}H_{22}O_4$	25.264	279.1578	Terpene lactone
40.	(+)-Mayurone	$C_{14}H_{22}O$	25.281	207.1736	ketone
41.	Docosanedioic acid	$C_{22}H_{42}O_4$	25.389	371.315	Alpha, omega-dicarboxylic acid and dicarboxylic fatty acid.
42.	Purine	$C_5H_4N_4$	25.793	121.0509	Purine
43.	6Z,9Z-Eicosadien-11-ol	$C_{20}H_{38}O$	26.007	312.3247	Aliphatic alcohol

Table 2 Total dry weight obtained from ZnO-NPs synthesis under different pH conditions

pH	Total dry weight (mg)
pH 3.24 (without NaOH)	41
pH 7	710
pH 9	773
pH 12	808

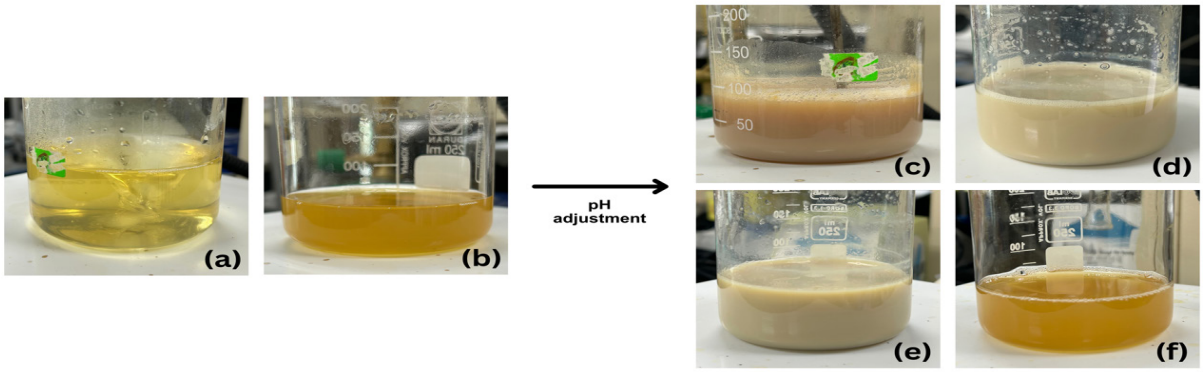

Fig. 3 Colour changes during ZnO-NP synthesis at different time **(a)** initial, **(b)** after 2 hours, **(c)** after adjusted to pH 12, **(d)** after adjusted to pH 9, **(e)** after adjusted to pH 7, and **(f)** without pH adjustment

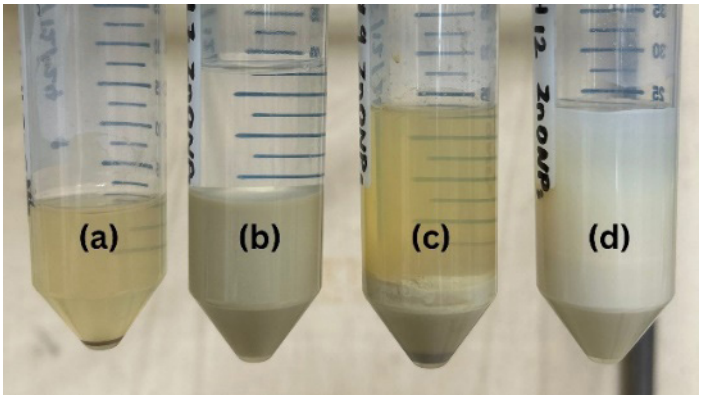

Fig. 4 Colloidal solutions of ZnO-NPs obtained after centrifugation and rinsing: **(a)** without NaOH, **(b)** pH 7, **(c)** pH 9, **(d)** pH 12

pH. The smallest Z-average size (131.1 nm) and the lowest PDI value (0.102) were observed at pH 12, suggesting good size uniformity in its colloidal suspension (Figs. 7 and 8). In contrast, ZnO-NPs synthesized without NaOH exhibited the largest average size (374.8 nm) and PDI value (0.355), indicating broader size distribution and poor NPs dispersion. However, the particle size measured via this method was larger compared to those obtained from SEM and XRD, which may suggest particle aggregation. Moreover, the DLS technique tends to overestimate the particle size, as it measures the hydrodynamic diameter, which may include aggregations within the suspension [28].

In terms of zeta potential, it provides an insight into the surface charge of ZnO-NPs, which represents their potential stability in colloidal suspension. According to previous studies, particles with zeta potential values greater than +30 mV or less than -30 mV typically form stable suspensions due to sufficient electrostatic repulsion, thereby preventing aggregation [29].

10.22036/ncr.2025.527594.1486
Nanochem Res, 2026, 11(1): 152-168

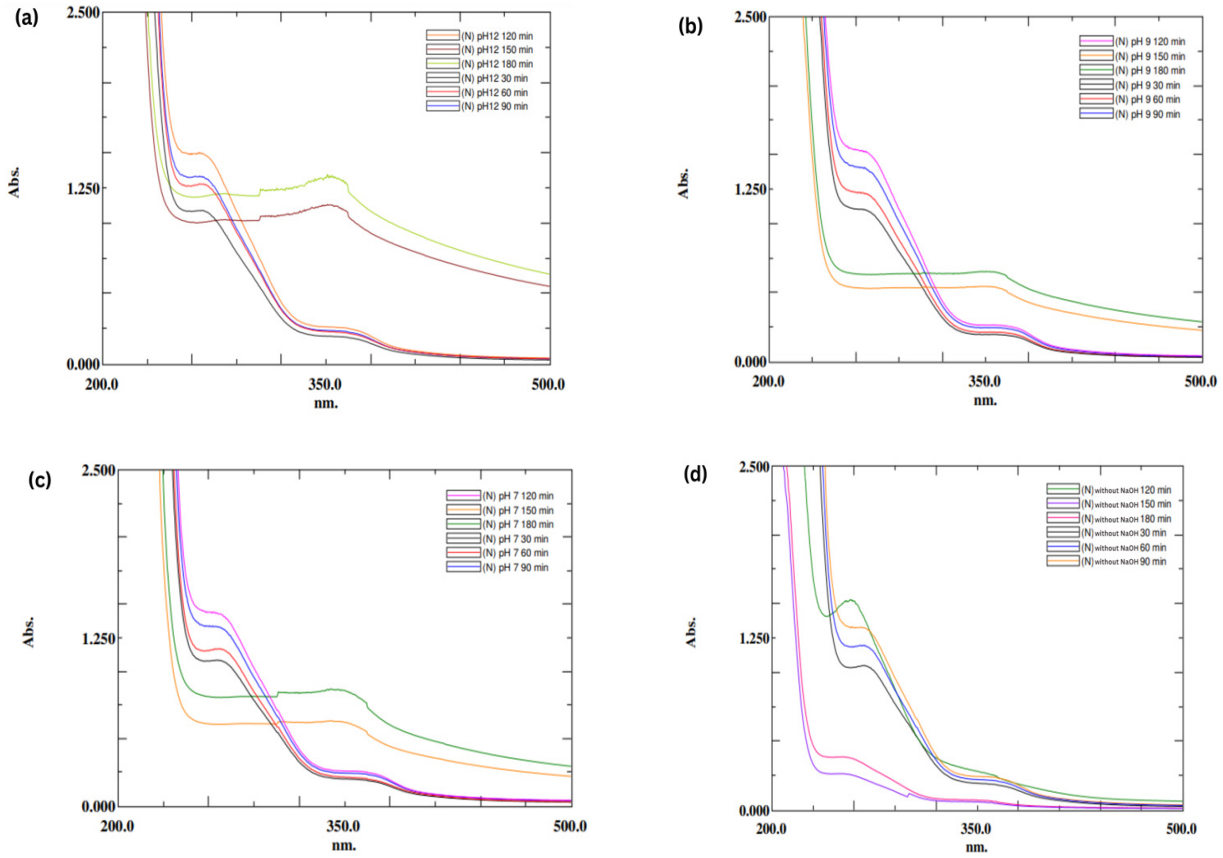

Fig. 5 UV-Vis spectrum of ZnO-NPs at every 30-minute intervals under **(a)** pH 12, **(b)** pH 9, **(c)** pH 7, and **(d)** without NaOH. Samples were diluted at a 1:20 ratio for 30, 60, 90, and 120 minutes, while a 1:100 ratio was used for 150 and 180 minutes.

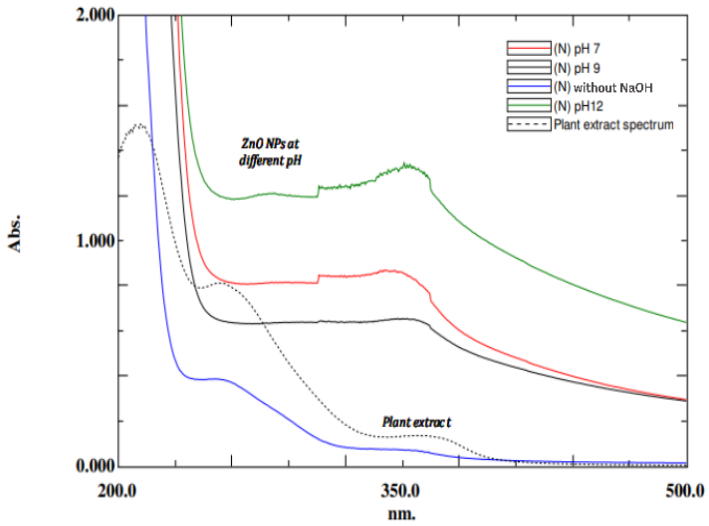

Fig. 6 Comparison of UV-Vis spectrum of ZnO-NPs at 180 minutes, synthesized under pH 12, 9, 7 and without NaOH, and plant extract

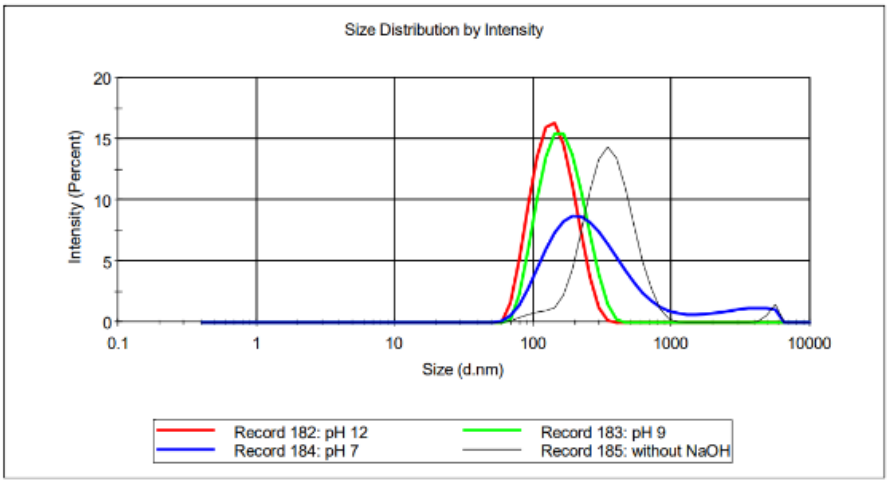

Fig. 7 Size distribution of ZnO-NPs synthesized under different pH conditions obtained from DLS

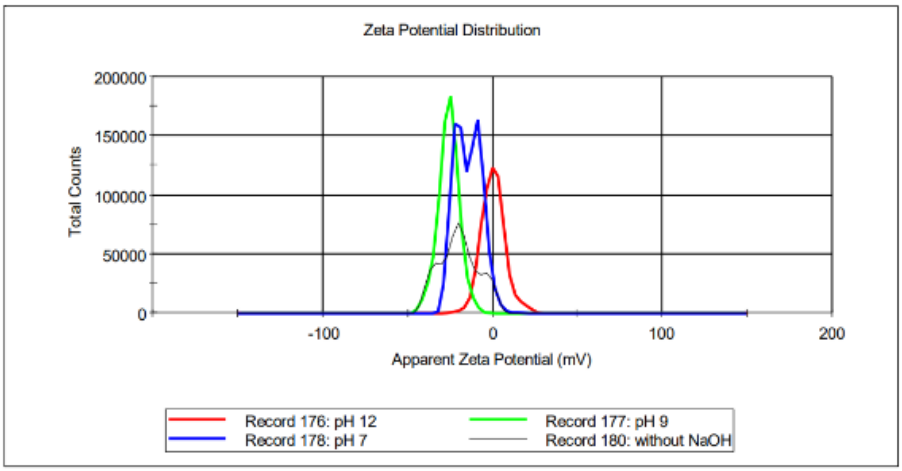

Fig. 8 Zeta potential distribution of ZnO-NPs synthesized under different pH conditions obtained from zeta potential analysis

In contrast, particles with low zeta potential values tend to aggregate due to the influence of Van der Waals forces between them. In this study, ZnO-NPs synthesized at all pH exhibited negative zeta potential values with magnitudes less negative than -30 mV (Table 3). This may suggest moderate colloidal stability of the NPs suspensions and explain the sedimentation observed at the bottom of the containers after some time. The negative surface charge is likely due to the adsorption of plant compounds onto the surface of NPs [18].

Based on the results of UV-Vis spectroscopy, DLS, and zeta potential analyses, pH 12 was identified as the optimal condition for ZnO-NP synthesis. Hence, the sample synthesized at this pH was selected for further characterisation.

3.3.3. FTIR analysis

FTIR analysis was conducted to confirm the formation of ZnO-NPs by identifying the Zn-O stretching bond which typically appears in the 600-400 cm^{-1} range [16] and to detect the potential functional groups from the plant extract that may be involved in the synthesis. Fig. 9 shows the FTIR spectrum of synthesized ZnO-NPs at pH 12 (Fig. 9a). A sharp peak detected at the lower energy region (500-400 cm^{-1}) may correspond to the Zn-O stretching bond, confirming the formation of ZnO-NPs. Besides that, three prominent absorption peaks were observed at 3392.14 cm^{-1}, 1372.61 cm^{-1}, and 892.08 cm^{-1}. The broad stretch peak at 3392.14 cm^{-1} and the weaker band at 1372.61 cm^{-1} may correspond to hydroxyl groups (OH) from alcohols, water, or phenolic compounds [18]. The band at 892.08 cm^{-1} could be attributed to C=C bending of alkenes, C-H bending of aromatics, or N-H of amines [10]. The similarity between these bands and those of the plant extract (3252.09 cm^{-1}, 1335.82

10.22036/ncr.2025.527594.1486
Nanochem Res, 2026, 11(1): 152-168

Table 3 Z-average, polydispersity index (PdI), and zeta potential values of ZnO-NPs synthesized under different pH conditions

pH	Z-average (d.nm)	PdI	Zeta potential (mV)
Without NaOH	374.8	0.355	-21.3
pH 7	229.6	0.347	-13.4
pH 9	149.0	0.106	-25.8
pH 12	131.1	0.102	-22.0

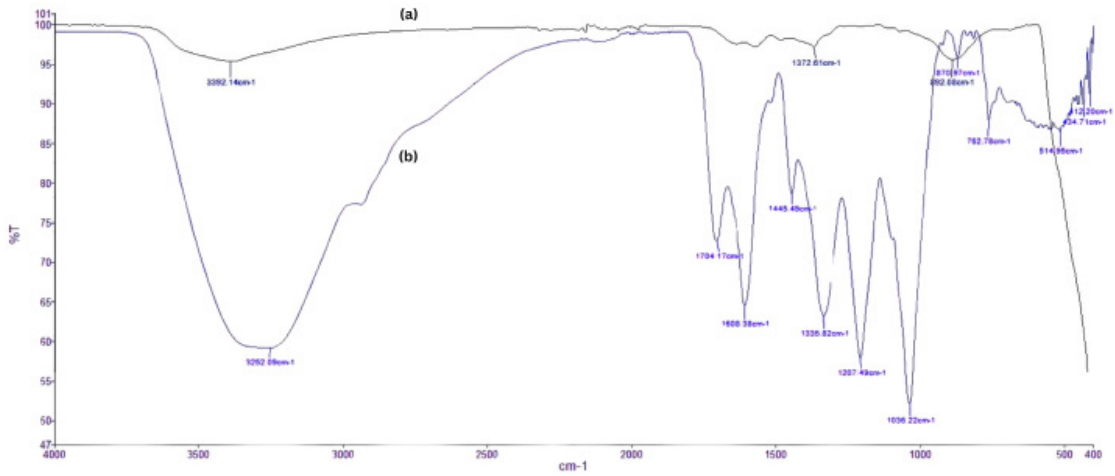

Fig. 9 FTIR spectra of **(a)** ZnO-NPs synthesized at pH 12, and **(b)** A. orthogyne extract obtained using ATR method

cm^{-1}, and 870.97 cm^{-1}) (Fig. 9b) may suggest the action of the plant extract as reducing and capping agents in the synthesis of ZnO-NPs.

Functional groups such as hydroxyl, carbonyl, and amine groups, present in plant biomolecules, including alkaloids, flavonoids, phenolics, aldehydes, ketones, protein, amino acids, carbohydrates, vitamins, saponins, tannins, and terpenoids, are known to contribute to the reduction of metal ion (Zn^{2+}) to their neutral metal atom (Zn^0) via donation of electrons, which subsequently leads to metal NPs formation [5,30]. Therefore, it can be speculated that phytochemicals, such as polyphenols and flavonoids found in *A. orthogyne* extract (Table 1), which contain OH groups, may have contributed to the bio-reduction of ZnO-NPs, as indicated by the presence of OH bands in the FTIR spectrum [31]. However, the relatively weak intensity of these peaks may suggest minimal involvement of the plant extract in the reduction process during synthesis, which aligns with the low total dry yield observed in the synthesis performed without the addition of NaOH.

3.3.4. SEM analysis

The morphology and size of the synthesized ZnO-NPs at pH 12 were examined using SEM analysis. As shown in Fig. 10, SEM images revealed that ZnO-NPs were aggregated and exhibited irregular particle shapes, which is similar to some observations reported in previous studies [10,32]. Additionally, SEM analysis also revealed smaller individual particle sizes, ranging between 50 and 90 nm, which were notably smaller than the sizes measured via DLS.

3.3.5. EDX analysis

In terms of elemental composition, EDX spectra (Table 4 and Fig. 11) revealed the presence of 71.92% zinc (Zn), 21.97% oxygen (O), 2.52% sodium (Na), and 3.55% carbon (C) elements. The presence of Zn and O as the dominant elements further confirms the formation of ZnO-NPs in this synthesis, while the presence of minor elements such as C and Na is due to the use of plant extract and the addition of NaOH for pH regulation during the synthesis.

3.3.6. XRD analysis

XRD analysis confirmed the crystalline structure of the synthesized ZnO-NPs. The diffractogram pattern (Fig. 12) exhibited sharp diffraction peaks at 2θ values of 31.81°, 34.45°, 36.3°, 47.57°, 56.62°, 62.84°, 66.37°, 67.93°, 69.07°, 72.49°, 76.92°, 81.37°, and 89.56°, which could be indexed to the (010), (002), (011), (012), (110), (013), (020), (112), (021), (004), (022), (014), and (023) crystal or lattice planes. The summary of the findings is tabulated in Table 5. This pattern

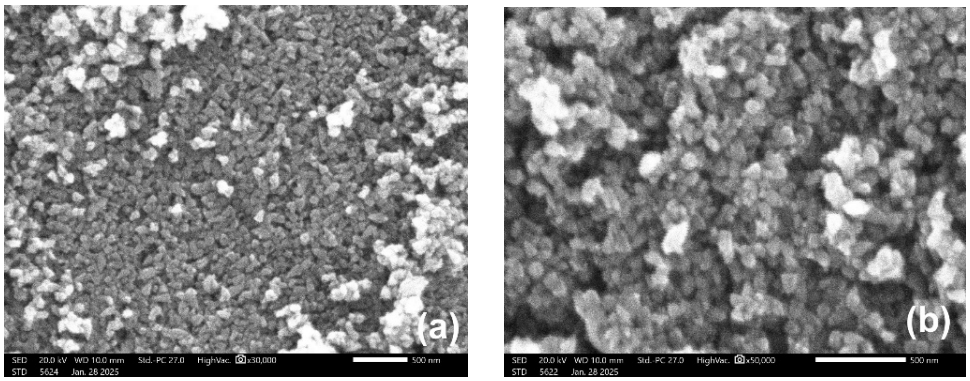

Fig. 10 Morphology of ZnO-NPs synthesized at pH 12 observed using SEM under different magnifications: **(a)** 30kx and **(b)** 50 kx

Table 4. Elemental composition of ZnO-NPs synthesized at pH 12 as well as their weight and atomic percentages obtained from EDX analysis

Element	Weight %	Atomic %
Zn	71.97	38.24
O	21.97	47.70
C	3.55	10.25
Na	2.52	3.80
Total	100.00	100.00

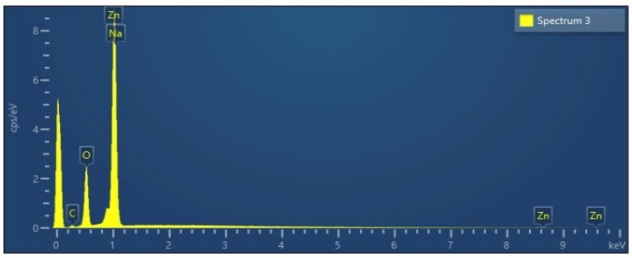

Spectrum 3				
Element	Line Type	Weight %	Weight % Sigma	Atomic %
C	K series	3.55	0.31	10.25
O	K series	21.97	0.22	47.70
Na	K series	2.52	0.40	3.80
Zn	L series	71.97	0.42	38.24
Total		100.00		100.00

Fig. 11 EDX spectra of ZnO-NPs synthesized at pH 12

aligns well with the ICSD Ref No. 98-065-6331, confirming the hexagonal wurtzite structure of the ZnO-NPs (Fakhari et al., 2019). The sharp and narrow diffraction peaks indicate the high crystallinity of the synthesized NPs, and the absence of extra peaks suggests no major impurities [10].

In this analysis, the mean crystallite size of ZnO-NPs was also calculated using the Debye-Scherrer equation (3),

$$D = \left(\frac{0.89\lambda}{\beta \cos\theta} \right) \quad (3)$$

where λ is the X-ray wavelength of Cu-Kα, β is the full width at half maxima (FWHM) of the diffraction peak (in radians), and θ is the Bragg angle (in degrees). Based on the results, the average crystallite size was found to range between 5 nm and 33.9 nm.

3.3.7. TGA analysis

Lastly, the TGA spectra of the synthesized ZnO-NPs (Fig. 13) demonstrated sample decomposition with increasing temperature. A total weight loss of 5.5 mg, or 5.5% of the initial 10 mg sample, was recorded between 30°C and 550°C. This

10.22036/ncr.2025.527594.1486
Nanochem Res, 2026, 11(1): 152-168

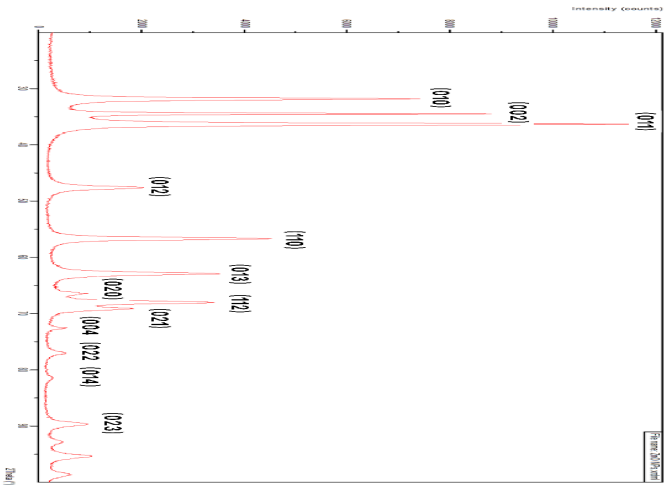

Fig. 12 XRD diffractogram pattern of ZnO-NPs synthesized at pH 12 with their lattice planes that align well with the ICSD Ref No. 98-065-6331

Table 5. °2θ values, hkl planes, d-spacing, FWHM left, and estimated crystalline size of ZnO-NPs synthesized at pH 12 obtained from XRD analysis

No.	Pos. (°2θ)	hkl plane	d-spacing (Å)	FWHM Left (°2θ)	Estimated crystalline size (nm)
1	31.8145	010	2.81048	0.4263	15.3
2	34.4494	002	2.60131	0.2639	33.9
3	36.2999	011	2.47283	0.4212	15.7
4	47.5718	012	1.90989	0.657	10.5
5	56.6185	110	1.62431	0.4864	14.2
6	62.8426	013	1.47757	0.6181	10.8
7	66.3678	020	1.40738	0.8143	7.1
8	67.9339	112	1.3787	0.5625	18.4
9	69.0689	021	1.35879	0.6354	10.8
10	72.4894	004	1.30286	1.131	5.0
11	76.9216	022	1.23846	0.9558	6.8
12	81.369	014	1.18163	1.0937	6.0
13	89.5604	023	1.09357	0.7998	13.6

weight reduction could be attributed to the removal of surface-adsorbed impurities, evaporation of adsorbed water, and decomposition of hydroxyls and residual organic materials from the plant extract [33,34]. However, a slight weight gain, around 0.2 mg, was observed above 550°C up to 700°C, resulting in a final residue weight of 9.47 mg. This increase may be caused by nitrogen gas absorption by the sample. Overall, the synthesized ZnO-NPs exhibited good thermal stability up to 700°C, with minimal weight loss not exceeding 5.5%.

3.3.8. Antimicrobial Assay

The antimicrobial activity of ZnO-NPs was evaluated against *Staphylococcus aureus, Bacillus subtilis, Escherichia coli, Pseudomonas aeruginosa,* and *Candida albicans* using the disc diffusion method, and the results are presented in Table 6. ZnO-NPs were assessed at four different concentrations: 0.5 mg/mL, 1.0 mg/mL, 3.0 mg/mL, and 5.0 mg/mL. Zones of

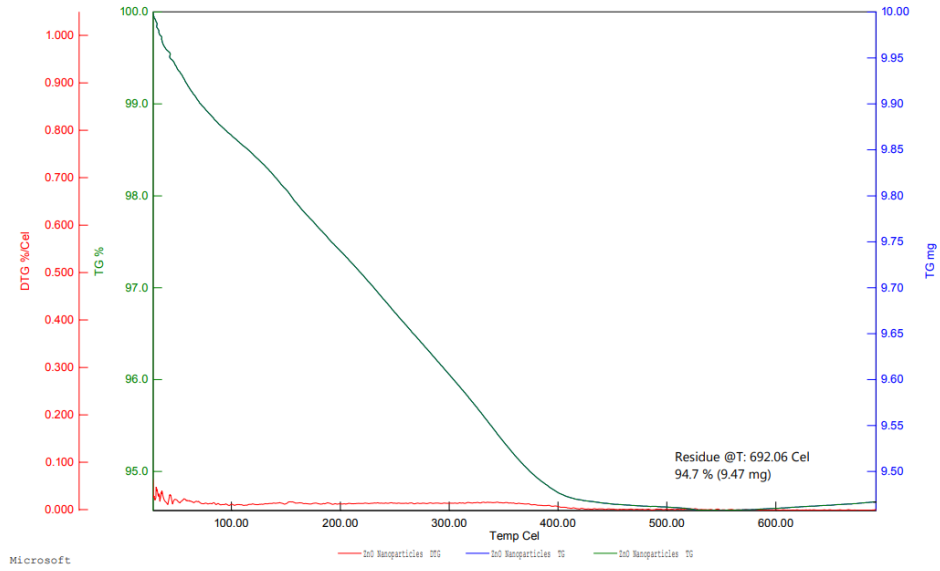

Fig. 13 TGA spectra of ZnO-NPs synthesized at pH 12

Table 6. Zone of inhibition exhibited by different samples against Staphylococcus aureus, Bacillus subtilis, Escherichia coli, Pseudomonas aeruginosa, and Candida albicans obtained via disc diffusion method. The results are represented as the mean values (mean ± SD) of two (n=2) replicates.

Treatments / Microorganisms	Zone of Inhibition (mm)				
	Staphylococcus aureus	Bacillus subtilis	Escherichia coli	Pseudomonas aeruginosa	Candida albicans
Positive control	17.0 ± 0.00	14.0 ± 0.71	11.0 0.00	16.0 ± 0.00	11.0 ± 1.41
Distilled water	0.00 ± 0.00	0.00 ± 0.00	0.00 ± 0.00	0.00 ± 0.00	0.00 ± 0.00
Zinc nitrate (5 mg/mL)	17.0 ± 0.00	9.00 ± 0.00	9.50 ± 2.12	8.50 ± 0.71	7.50 ± 5.30
Plant extract (5 mg/mL)	0.00 ± 0.00	0.00 ± 0.00	0.00 ± 0.00	0.00 ± 0.00	0.00 ± 0.00
ZnO-NPs (0.5 mg/mL)	0.00 ± 0.00	0.00 ± 0.00	0.00 ± 0.00	0.00 ± 0.00	NA
ZnO-NPs (1 mg/mL)	0.00 ± 0.00	0.00 ± 0.00	0.00 ± 0.00	0.00 ± 0.00	NA
ZnO-NPs (3 mg/mL)	7.50 ± 0.71	8.50 ± 0.71	8.00 ± 0.00	8.00 ± 0.00	NA
ZnO-NPs (5 mg/mL)	8.50 ± 0.71	9.00 ± 0.00	8.50 ± 0.71	8.00 ± 0.00	0.00 ± 0.00
ZnO-NPs (10 mg/mL)	NA	NA	NA	NA	7.75 ± 0.35

inhibition were observed only at 3.0 mg/mL and 5.0 mg/mL for all tested bacterial strains, indicating a dose-dependent effect. For *Candida albicans,* the fungal strain, the zone of inhibition was observed at a higher concentration of 10 mg/mL.

Compared to the positive control (amoxicillin 30 µg/disc and econazole 100 µg/mL), ZnO-NPs exhibited significantly smaller zones of inhibition, even at higher concentrations, suggesting a relatively lower antimicrobial potency than standard antimicrobial drugs. On the other hand, zinc nitrate (5 mg/mL) demonstrated moderate inhibitory activity, while *A. orthogyne* leaf extract and distilled water produced no antimicrobial activities. Visual observations of the inhibitory zones are shown in Figure 14.

The antimicrobial activity of ZnO-NPs is mainly attributed to their ability to induce oxidative stress in microbial cells through the generation of ROS [35,36]. Besides that, ZnO-

10.22036/ncr.2025.527594.1486
Nanochem Res, 2026, 11(1): 152-168

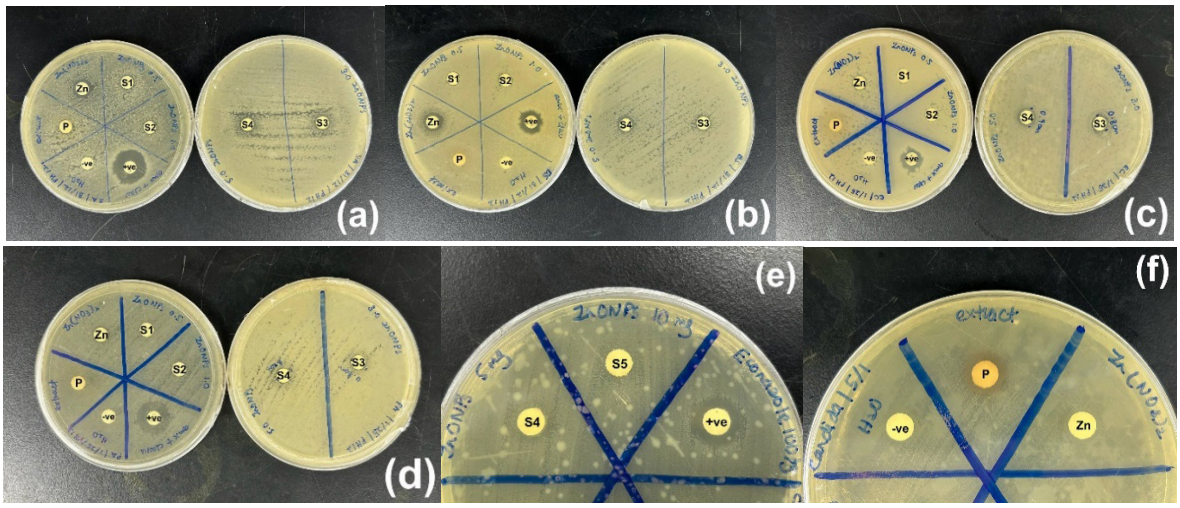

Fig. 14. Patterns of zone of inhibition exhibited by ZnO-NPs at different concentration against different types of organisms obtained via disc diffusion method**.** (+ve: positive control, -ve: negative control, Zn: zinc nitrate hexahydrate (5 mg/mL), P: plant extract (5 mg/mL), S1: ZnO-NPs (0.5 mg/mL), S2: ZnO-NPs (1 mg/mL), S3: ZnO-NPs (3 mg/mL), S4: ZnO-NPs (5 mg/mL), S5: ZnO-NPs (10 mg/mL))

Table 7. Percentage of cell viability of MCF-7 cell lines after 24 hours of exposure towards three different types of treatments at different concentrations and their IC50 values obtained via MTT assay. The results are represented as the mean values (mean ± SD) of three (n = 3) replicates.

Samples	Concentrations (mg/mL)						IC_{50} (mg/mL)
	0.031	0.063	0.125	0.25	0.5	1.0	
ZnO-NPs	97.29 ± 4.96	91.07 ± 8.17	86.53 ± 8.59	30.75 ± 4.39	25.24 ± 4.87	9.93 ± 0.61	0.2246
Tamoxifen	72.34 ± 1.52	70.76 ± 5.44	49.31 ± 1.40	7.34 ± 1.19	9.39 ± 0.96	6.22 ± 0.15	0.0955
Zn Nitrate	29.25 ± 3.94	32.09 ± 3.93	22.93 ± 3.06	18.85 ± 3.87	13.61 ± 0.31	12.98 ± 4.77	0.0013

NPs may penetrate the microbial cell membrane, disrupt intracellular structures and functions, and eventually inhibit cell growth and proliferation [7,37]. Additionally, it may also disrupt the integrity and permeability of the cell membranes, leading to cellular contents leakage and cell death [35]. These mechanisms are strongly influenced by the size of the NPs. Smaller particles provide a larger surface area for interaction, enhancing both ROS generation and antimicrobial contact. Thus, the size of NPs plays a crucial role in determining their antimicrobial effectiveness.

In this study, higher concentrations were required for ZnO-NPs to exert antimicrobial activities compared to previous studies. For instance, ZnO-NPs synthesized using *Ocimum americanum,* with an average size of 21 nm in colloidal form, demonstrated superior antimicrobial activity at just 50 µg/mL, surpassing the activity of positive controls, gentamicin 10 µg/disc and nystatin 100 U/disc [18]. In contrast, a higher MIC concentration (1.5-2.5 mg/mL) was reported for ZnO-NPs synthesized using *Lactobacillus plantarum* TA4 with an average size of 292.6 nm in colloids [38]. Hence, the reduced efficacy and higher concentration requirement of the synthesized ZnO-NPs in this study are likely due to the larger average colloidal size (131.1 nm) and particle aggregation, as confirmed by SEM.

3.3.9. Cytotoxic Assay

The cytotoxicity effect of ZnO-NPs, tamoxifen and zinc nitrate hexahydrate was evaluated against MCF-7 breast cancer cell lines. Table 7 presents the percentage of cell viability after 24 hours of treatment with each sample at different concentrations. Based on the results, all three samples showed a significant reduction in cell viability ($p < 0.05$), with no statistically significant differences in their potencies ($p > 0.05$) when compared using one-way ANOVA, suggesting comparable cytotoxicity efficacy between them.

Other than that, zinc nitrate hexahydrate exhibited the lowest IC_{50} value (0.0013 mg/mL), followed by tamoxifen (0.0955 mg/mL) and ZnO-NPs (0.2246 mg/mL). The IC_{50} values represent the concentrations required to induce a 50%

cytotoxic effect against MCF-7 cells. The lower the IC_{50} value, the higher the cytotoxic potential. Therefore, in this study, zinc nitrate hexahydrate demonstrated the greatest cytotoxic effect among the samples. To further support these findings, the treated cells were observed under an inverted microscope. Cells treated with ZnO-NPs, tamoxifen, and zinc nitrate displayed notable morphological changes, including loss of defined shape, compared to the untreated control.

Additionally, the cytotoxicity of *A. orthogyne* leaf extract was also evaluated, but not in serial dilutions for IC_{50} determination. At 5 mg/mL concentration, the extract depicted a moderate cytotoxic effect, resulting in a 35.32% reduction in cell viability after 24 hours of treatment.

A similar cytotoxic profile of green-synthesized ZnO-NPs has been reported in previous studies against MCF-7, as well as other cancer cell lines such as hepatocellular carcinoma (Hep-G2, Huh-7), lung cancer (A-549, H460), and breast cancer (MDA-MB-231) [39]. These findings support the potential of ZnO-NPs as a promising alternative to the current cancer therapies. However, in the present study, the cytotoxicity of *A. orthogyne*-mediated ZnO-NPs was only evaluated against the MCF-7 cancer cell line without assessing their effects against normal cells. Thus, the safety profile of these NPs remains unclear.

According to existing literature, several in vitro studies have demonstrated the selective cytotoxic effect of ZnO-NPs towards cancerous cells, suggesting its minimal toxicity towards normal healthy cells [40]. For instance, ZnO-NPs synthesized using *Euphorbia retusa* extract showed an IC_{50} value >100 µg/mL against the normal fibroblast cells (WI-38), while exhibiting lower IC_{50} values against tumour cell lines, including HePG-2 (31.75 µg/mL), MCF-7 (30.05 µg/mL), and PC3 (16.04 µg/mL) [39]. This selectivity is attributed to the enhanced permeability and retention (EPR) effect in tumour tissues compared to normal tissues [40], caused by the leaky vasculature and poor lymphatic drainage surrounding the tumour cells, which facilitate accumulation and diffusion of nanoparticles into the tumour cells [40]. Moreover, the tumour cells also typically generate larger amounts of ROS due to their active metabolic activity [40]. Therefore, with additional ROS generated by ZnO-NPs, it will intensify the oxidative stress in the tumour cells, leading to apoptosis while exerting less damage to normal cells. In addition, the anticancer mechanism of ZnO-NPs has also been studied via the immunoblotting method, which showed increased expression of caspase-8, an apoptosis-related enzyme that promotes programmed cell death during normal cell development, and decreased expression of COX-2, a protein that helps in the proliferation, inflammation, and metastasis of cancerous cells [41].

To sum up, these results highlight the potential of the synthesized ZnO-NPs as a selective and effective anticancer agent. Nonetheless, further research involving normal cells and in vivo models is required to fully establish their safety profile and therapeutic application.

3.3.10. Limitations

Despite the valuable findings, this study presents several limitations that may influence the interpretation of the results. Firstly, although LC-MS analysis successfully identified multiple phytoconstituents of *A. orthogyne* leaf extract, further phytochemical evaluations such as total phenolic content and antioxidant activity were not conducted. This limits the understanding of the plant's role in the ZnO-NPs synthesis and raises questions about its true effectiveness in this green synthesis, especially when NaOH appeared to have a more dominant effect on the ZnO-NPs formation than the plant extract. Secondly, the method optimisation was only limited to pH, without testing other factors such as temperature, extract-to-precursor ratios, and reaction time, which may affect the stability and yield of the NPs. Therefore, the current synthesis conditions may not produce the most stable NPs and may not reflect the real potential of the plant in assisting NPs formation. Thirdly, the antimicrobial assay was performed in duplicates instead of triplicates due to limited resources and time constraints, which may reduce the statistical confidence and reproducibility of the results obtained. Lastly, the safety profile of the synthesized ZnO-NPs was not evaluated against normal cell lines. As a result, the selectivity of their cytotoxicity, which is important before making an anticancer claim, cannot be determined. Hence, these limitations should be considered when interpreting the findings and should be addressed in future research to enhance the reliability, robustness, and applicability of the results.

4. CONCLUSION

In conclusion, ZnO-NPs were successfully synthesized using *A. orthogyne* extract with the aid of NaOH. The synthesis was carried out under various pH conditions to determine the optimal pH for ZnO-NPs formation. pH 12 was found to be the most favourable pH, yielding the smallest particle size with good dispersion. FTIR analysis confirmed the role of the plant extract as a reducing and capping agent as well as the successful formation of ZnO-NPs. UV-Vis spectroscopy revealed absorption peaks at approximately 265 nm in the absence of NaOH and 351 nm when NaOH was added. DLS and zeta potential analyses revealed a well-dispersed colloid with the smallest particle size (131.1 nm) and negative surface charge at pH 12. SEM images showed agglomerated particles with irregular shapes, while XRD confirmed the hexagonal wurtzite structure of ZnO-NPs. TGA analysis indicated good thermal stability of the synthesized NPs up to 700°C, with minimal weight loss not exceeding 5.5%. Moreover, the synthesized ZnO-NPs indicated potential antimicrobial activity against

10.22036/ncr.2025.527594.1486
Nanochem Res, 2026, 11(1): 152-168

all bacterial and fungal strains, as well as significant cytotoxic activity on the MCF-7 cell line. These findings highlight *A. orthogyne* extract as a promising, eco-friendly approach for synthesising ZnO-NPs with potential applications in antimicrobial and cytotoxic areas. However, future research is needed to optimize the synthesis conditions, especially to reduce the pH dependency while improving the properties of the NPs.

Acknowledgements
The authors are grateful to the Department of Pharmaceutical Technology, Kulliyyah of Pharmacy, IIUM Kuantan Campus for providing research facilities. The authors also thank Kulliyyah of Medicine, IIUM Kuantan Campus and Mdm Zurina Mahmud for her help in providing fees for SEM, XRD, and TGA analysis.

Data availability statements
No datasets were generated or analyzed during the current study.

Authors contributions
Methodology, N.M.; conducted the research and collected the data, N.M.; writing—original draft preparation, N.M; supervision, M.T., J.M.J; funding acquisition, J.M.J, J.K. and M.T; review, D.S., M.T.,
M.F. and M.S.H. All authors have read and agreed to the published version of the manuscript.

Conflict of interest
The authors declare no conflicts of interest.

Funding
No funding was received in concducting this study.

REFERENCES

1. WHO. Antimicrobial resistance [Internet]. 2023.
2. WHO. Global antimicrobial resistance and use surveillance system (GLASS) report: 2022 [Internet]. 2022.
3. Shkodenko L, Kassirov I, Koshel E. Metal Oxide Nanoparticles Against Bacterial Biofilms: Perspectives and Limitations. Microorganisms [Internet]. 2020; 8(10). https://doi.org/10.3390/microorganisms8101545
4. Muhammad MH, Idris AL, Fan X, Guo Y, Yu Y, Jin X, et al. Beyond Risk: Bacterial Biofilms and Their Regulating Approaches. 2020;Volume 11 - 2020. https://doi.org/10.3389/fmicb.2020.00928
5. Susanti D, Haris MS, Taher M, Khotib J. Natural Products-Based Metallic Nanoparticles as Antimicrobial Agents. 2022;Volume 13 - 2022. https://doi.org/10.3389/fphar.2022.895616
6. Zhao A, Sun J, Liu Y. Understanding bacterial biofilms: From definition to treatment strategies. 2023;Volume 13 - 2023. https://doi.org/10.3389/fcimb.2023.1137947
7. Ahamad Khan M, Lone SA, Shahid M, Zeyad MT, Syed A, Ehtram A, et al. Phytogenically Synthesized Zinc Oxide Nanoparticles (ZnO-NPs) Potentially Inhibit the Bacterial Pathogens: In Vitro Studies. Toxics [Internet]. 2023; 11(5). https://doi.org/10.3390/toxics11050452
8. Gudkov SV, Burmistrov DE, Serov DA, Rebezov MB, Semenova AA, Lisitsyn AB. A Mini Review of Antibacterial Properties of ZnO Nanoparticles. 2021;Volume 9 - 2021. https://doi.org/10.3389/fphy.2021.641481
9. Murali M, Kalegowda N, Gowtham HG, Ansari MA, Alomary MN, Alghamdi S, et al. Plant-Mediated Zinc Oxide Nanoparticles: Advances in the New Millennium towards Understanding Their Therapeutic Role in Biomedical Applications. Pharmaceutics [Internet]. 2021; 13(10). https://doi.org/10.3390/pharmaceutics13101662
10. Ifeanyichukwu UL, Fayemi OE, Ateba CN. Green Synthesis of Zinc Oxide Nanoparticles from Pomegranate (Punica granatum) Extracts and Characterization of Their Antibacterial Activity. Molecules [Internet]. 2020; 25(19). https://doi.org/10.3390/molecules25194521
11. Asif N, Amir M, Fatma T. Recent advances in the synthesis, characterization and biomedical applications of zinc oxide nanoparticles. Bioprocess and Biosystems Engineering. 2023;46(10):1377-98. https://doi.org/10.1007/s00449-023-02886-1
12. Agarwal H, Venkat Kumar S, Rajeshkumar S. A review on green synthesis of zinc oxide nanoparticles - An eco-friendly approach. Resource-Efficient Technologies. 2017;3(4):406-13. https://doi.org/10.1016/j.reffit.2017.03.002
13. Nguyen-Ngoc H, Le-Thi-Phuong T, Vu-Van T, Pham-Ha-Thanh T, Nguyen-Huu T. Phytochemical and Pharmacological Review of the Genus Antidesma. Natural Product Communications. 2024;19(4):1934578X241247990. https://doi.org/10.1177/1934578X241247990
14. Yasser M, Rafi M, Wahyuni WT, Asfar AMIA, Widiyanti SE. Total Phenolic Content of Methanol Extract from Buni Fruits (Antidesma bunius L.) Water. Journal of Physics: Conference Series. 2020;1655(1):012029. https://doi.org/10.1088/1742-6596/1655/1/012029
15. Ahmed NA, Othman AS. Green fabrication of ZnO nanoparticles via spirulina platensis and its efficiency against biofilm forming pathogens. Microbial Cell Factories. 2024;23(1):92. https://doi.org/10.1186/s12934-024-02360-x
16. Fakhari S, Jamzad M, Kabiri Fard H. Green synthesis of zinc oxide nanoparticles: a comparison. Green Chemistry Letters and Reviews. 2019;12(1):19-24. https://doi.org/10.1080/17518253.2018.1547925
17. Vidhya E, Vijayakumar S, Prathipkumar S, Praseetha PK. Green way biosynthesis: Characterization, antimicrobial and anticancer activity of ZnO nanoparticles. Gene Reports. 2020;20:100688. https://doi.org/10.1016/j.genrep.2020.100688
18. Narendra Kumar HK, Chandra Mohana N, Nuthan BR, Ramesha KP, Rakshith D, Geetha N, et al. Phyto-mediated synthesis of zinc oxide nanoparticles using aqueous plant extract of Ocimum americanum and evaluation of its bioactivity. SN Applied Sciences. 2019;1(6):651. https://doi.org/10.1007/s42452-019-0671-5
19. Mthana MS, Mthiyane MN, Ekennia AC, Singh M, Onwudiwe DC. Cytotoxicity and antibacterial effects of silver doped zinc oxide nanoparticles prepared using fruit extract of Capsicum Chinense. Scientific African. 2022;17:e01365. https://doi.org/10.1016/j.sciaf.2022.e01365
20. Dhandapani KV, Anbumani D, Gandhi AD, Annamalai P, Muthuvenkatachalam BS, Kavitha P, et al. Green route for the synthesis of zinc oxide nanoparticles from Melia azedarach leaf extract and evaluation of their antioxidant and antibacterial

activities. Biocatalysis and Agricultural Biotechnology. 2020;24:101517. https://doi.org/10.1016/j.bcab.2020.101517
21. Asmat-Campos D, López-Medina E, Montes de Oca-Vásquez G, Gil-Rivero E, Delfín-Narciso D, Juárez-Cortijo L, et al. ZnO Nanoparticles Obtained by Green Synthesis as an Alternative to Improve the Germination Characteristics of L. esculentum. Molecules [Internet]. 2022; 27(7). https://doi.org/10.3390/molecules27072343
22. Bandeira M, Giovanela M, Roesch-Ely M, Devine DM, da Silva Crespo J. Green synthesis of zinc oxide nanoparticles: A review of the synthesis methodology and mechanism of formation. Sustainable Chemistry and Pharmacy. 2020;15:100223. https://doi.org/10.1016/j.scp.2020.100223
23. Fadhillah IR, Taher M, Nur M, Susanti D. Green Synthesized of Silver Nanoparticles from Anisophyllea corneri Leaf Extract and Its Antimicrobial and Cytotoxic Activities. Journal of Pharmacy. 2024;4(1):103-15. https://doi.org/10.31436/jop.v4i1.265
24. Abdelmigid HM, Hussien NA, Alyamani AA, Morsi MM, AlSufyani NM, kadi HA. Green Synthesis of Zinc Oxide Nanoparticles Using Pomegranate Fruit Peel and Solid Coffee Grounds vs. Chemical Method of Synthesis, with Their Biocompatibility and Antibacterial Properties Investigation. Molecules [Internet]. 2022; 27(4). https://doi.org/10.3390/molecules27041236
25. Rana A, Yadav K, Jagadevan S. A comprehensive review on green synthesis of nature-inspired metal nanoparticles: Mechanism, application and toxicity. Journal of Cleaner Production. 2020;272:122880. https://doi.org/10.1016/j.jclepro.2020.122880
26. Radulescu D-M, Surdu V-A, Ficai A, Ficai D, Grumezescu A-M, Andronescu E. Green Synthesis of Metal and Metal Oxide Nanoparticles: A Review of the Principles and Biomedical Applications. International Journal of Molecular Sciences [Internet]. 2023; 24(20). https://doi.org/10.3390/ijms242015397
27. Doğan SŞ, Kocabaş A. Green synthesis of ZnO nanoparticles with Veronica multifida and their antibiofilm activity. Human & Experimental Toxicology. 2019;39(3):319-27. https://doi.org/10.1177/0960327119888270
28. Faisal S, Jan H, Shah SA, Shah S, Khan A, Akbar MT, et al. Green Synthesis of Zinc Oxide (ZnO) Nanoparticles Using Aqueous Fruit Extracts of Myristica fragrans: Their Characterizations and Biological and Environmental Applications. ACS Omega. 2021;6(14):9709-22. https://doi.org/10.1021/acsomega.1c00310
29. Okaiyeto K, Gigliobianco MR, Di Martino P. Biogenic Zinc Oxide Nanoparticles as a Promising Antibacterial Agent: Synthesis and Characterization. International Journal of Molecular Sciences [Internet]. 2024; 25(17). https://doi.org/10.3390/ijms25179500
30. Meer B, Andleeb A, Iqbal J, Ashraf H, Meer K, Ali JS, et al. Bio-Assisted Synthesis and Characterization of Zinc Oxide Nanoparticles from Lepidium sativum and Their Potent Antioxidant, Antibacterial and Anticancer Activities. Biomolecules [Internet]. 2022; 12(6). https://doi.org/10.3390/biom12060855
31. Rajeshkumar S, Parameswari RP, Sandhiya D, Al-Ghanim KA, Nicoletti M, Govindarajan M. Green Synthesis, Characterization and Bioactivity of Mangifera indica Seed-Wrapped Zinc Oxide Nanoparticles. Molecules [Internet]. 2023; 28(6). https://doi.org/10.3390/molecules28062818
32. Umar H, Kavaz D, Rizaner N. Biosynthesis of zinc oxide nanoparticles using Albizia lebbeck stem bark, and evaluation of its antimicrobial, antioxidant, and cytotoxic activities on human breast cancer cell lines. International Journal of Nanomedicine. 2019;14(null):87-100. https://doi.org/10.2147/IJN.S186888
33. Khan AU, Malik N, Singh B, Ansari NH, Rehman M, Yadav A. Biosynthesis, and characterization of Zinc oxide nanoparticles (ZnONPs) obtained from the extract of waste of strawberry. Journal of Umm Al-Qura University for Applied Sciences. 2023;9(3):268-75. https://doi.org/10.1007/s43994-023-00038-5
34. Hassan H, Elkady M, el-sayed E, Hamed AM, Hussein AM, Mahmoud IM. Synthesis and characterization of zinc oxide nanoparticles using green and chemical synthesis techniques for phenol decontamination. International Journal of Nanoelectronics and Materials. 2018;11:179-94.
35. Huq MA, Apu MA, Ashrafudoulla M, Rahman MM, Parvez MA, Balusamy SR, et al. Bioactive ZnO Nanoparticles: Biosynthesis, Characterization and Potential Antimicrobial Applications. Pharmaceutics [Internet]. 2023; 15(11). https://doi.org/10.3390/pharmaceutics15112634
36. Jiang J, Pi J, Cai J. The Advancing of Zinc Oxide Nanoparticles for Biomedical Applications. Bioinorganic Chemistry and Applications. 2018;2018(1):1062562. https://doi.org/10.1155/2018/1062562
37. Sirelkhatim A, Mahmud S, Seeni A, Kaus NHM, Ann LC, Bakhori SKM, et al. Review on Zinc Oxide Nanoparticles: Antibacterial Activity and Toxicity Mechanism. Nano-Micro Letters. 2015;7(3):219-42. https://doi.org/10.1007/s40820-015-0040-x
38. Mohd Yusof H, Abdul Rahman NA, Mohamad R, Zaidan UH, Samsudin AA. Biosynthesis of zinc oxide nanoparticles by cell-biomass and supernatant of Lactobacillus plantarum TA4 and its antibacterial and biocompatibility properties. Scientific Reports. 2020;10(1):19996. https://doi.org/10.1038/s41598-020-76402-w
39. Abduljabbar B, El-Zayat M, El-Amier Y, El-Halawany E-S. Biosynthesis, characterization, and cytotoxic activities of zinc nanoparticles (ZnNPs) using Euphorbia retusa extract. Kuwait Journal of Science. 2024;51(1):100108. https://doi.org/10.1016/j.kjs.2023.08.001
40. Bisht G, Rayamajhi S. ZnO Nanoparticles: A Promising Anticancer Agent. Nanobiomedicine. 2016;3:9. https://doi.org/10.5772/63437
41. Alqahtani AA, Attia GH, Elgamal A, Aleraky M, Youns M, Ibrahim AM, et al. Cytotoxic Activity of Zinc Oxide Nanoparticles Mediated by Euphorbia Retusa. Crystals [Internet]. 2022; 12(7). https://doi.org/10.3390/cryst12070903